Efficiency Analysis of the Wave-to-Grid Energy Conversion of the UniWave200 Wave Energy Converter

Fadia Ticona Rollano, Arthur Santos, Robert J. Cavagnaro, *Member, IEEE*, Scott Hunter, and Tom Denniss

***Abstract*—Wave energy is a vast and largely untapped resource with the potential to contribute significantly to global energy production. A new wave energy technology has been developed by an Australian company, Wave Swell Energy Ltd., consisting of a unique unidirectional axial turbine version of the well-established oscillating water column (OWC) concept. A full-scale prototype of the technology, the UniWave200, was deployed for grid-connected testing near the coastline of King Island, Tasmania, from 2021 to 2022. Data collected during the pilot project were analyzed by the US Department of Energy's Pacific Northwest National Laboratory (PNNL). The results of this analysis indicate the full-process wave-to-grid energy conversion efficiency, based on the combined capture width ratio (CWR) and power take-off (PTO) efficiency, to be on the order of 45% for significant wave heights above 1 m.**

***Index Terms*—Capture width ratio, efficiency analysis, field test, grid-connected, oscillating water column, power take-off efficiency, wave energy, wave energy converter.**

I. Introduction

ONE of the largest underutilized renewable energy resources is wave energy, which could provide a significant supply to the electric grid worldwide. Estimates of global resources available along coastlines are in the range of 1–2 $\times$ 10^4 TWh/yr when considering the directionality of the incident waves [1], [2]. Unlike other renewable technology sectors such as solar, wind, and tidal, all of which have tended to converge on technological solutions with limited variability, the range of wave energy technologies remains diverse. The variability in the characteristics of waves (e.g., height, period, and direction), driven by diverse geospatial conditions, has naturally resulted in a suite of technology topologies and designs tailored to classes of resource and tuned to resonate with incoming waves [3].

A plethora of wave energy technologies continue to be investigated throughout the world, some of which are new, while others are incremental improvements on concepts that have been in existence for several decades. A recent technology review [4] highlighted the challenges facing continued development, noting the small cumulative power-generating capacity of the industry and no demonstrations of cost-competitive electricity generation at a commercial scale. This reality makes it difficult to clearly define a "state of the art" for the sector. However, progress is being made that suggests that wave energy could become a cost-effective and meaningful complement to other more mature renewable generation technologies.

One of the most established concepts in the field of wave energy is that of the oscillating water column (OWC), a technology first commercialized in the 1960s as a means of powering navigation buoys [5]. An OWC is a form of artificial blowhole, comprising a large chamber with an opening below the waterline that generally faces in the direction of the incoming waves. The waves drive a column of water inside the OWC chamber to rise and fall, displacing the air above it, which in turn drives an air turbine to generate electricity.

The vast majority of OWC prototypes have a bidirectional or self-rectifying form, with air passing the turbine on both the upstroke of the wave (air leaving the chamber) and the downstroke (air being pulled back into the chamber) [6]. This requires a turbine that is capable of operating with a reversing airflow and requires flow-direction symmetry, which can be achieved with fixed blades having a symmetric airfoil profile or guide vanes at the expense of aerodynamic efficiency. More complex variable-pitch designs may offer benefits including their response to changing flow conditions with trade-offs for simplicity and overall aerodynamic conversion efficiency [7]. Examples of turbines used in bidirectional OWCs include the Wells, Setoguchi, HydroAir, Denniss-Auld, and biradial impulse varieties. Most have been of the axial flow type [8], [9], [10].

While blade twist has been an important aspect of more traditional unidirectional flow turbines (as well as propellers, impellers, etc.) that have been developed over the past century

Received 7 February 2024; revised 6 June 2024, 25 August 2024, and 24 September 2024; accepted 25 September 2024. Date of publication 17 October 2024; date of current version 24 March 2025. The demonstration field test was partially funded by the Australian Renewable Energy Agency (ARENA). The analysis of the data provided to Pacific Northwest National Laboratory by Wave Swell Energy Ltd. was supported by the United States Department of Energy, Office of Energy Efficiency and Renewable Energy, Water Power Technologies Office under contract DE-AC05-76RL01830. Paper no. TSTE-00190-2024. *(Corresponding author: Fadia Ticona Rollano.)*

Fadia Ticona Rollano and Robert J. Cavagnaro are with Pacific Northwest National Laboratory, Seattle, WA 98109 USA (e-mail: fadia.ticonar@pnnl.gov; robert.cavagnaro@pnnl.gov).

Arthur Santos was with Pacific Northwest National Laboratory, Richland, WA 99354 USA. He is now with CSU Energy Institute, Fort Collins, CO 80524 USA (e-mail: arthur.santos@colostate.edu).

Scott Hunter and Tom Denniss are with Wave Swell Energy Ltd., Melbourne, VIC 3000, Australia (e-mail: scott.hunter@waveswell.com; tom.denniss@waveswell.com).

Color versions of one or more figures in this article are available at https://doi.org/10.1109/TSTE.2024.3483655.

Digital Object Identifier 10.1109/TSTE.2024.3483655

© 2024 The Authors. This work is licensed under a Creative Commons Attribution 4.0 License. For more information, see https://creativecommons.org/licenses/by/4.0/

or more, the symmetry requirements of bidirectional turbines preclude the use of it. Blade twist is used to optimize the angle of attack of the flow along the blade's length from root to tip and, consequently, provides a significantly higher aerodynamic conversion efficiency than that achieved with non-twisted blades. The symmetry requirements of bidirectional turbines also demand that both ends of the turbine blades have leading edge profiles, further reducing the magnitude of the conversion efficiency. In essence, a unidirectional axial flow turbine has an inherently greater propensity for aerodynamic conversion efficiency than does a bidirectional axial flow turbine.

Despite decades of research and development, large-scale sea trials of wave energy converters (WECs) remain rare. Of the roughly 70 studies utilized by Babarit in compiling a database of published WEC performance information as of 2015, only a single device with its set of results is classified as a sea trial [11]. Subsequently, several more performance results have been documented and published, including for the Mutriku and Pico fixed OWC wave power plants [12], [13]. The characterization of WEC performance in real ocean conditions and with a connection to the grid is crucial for developers to demonstrate technology readiness. The publication of these performance results once obtained advances the industry by providing real-world benchmarks to which smaller-scale prototype, tank, and numerical model testing may be compared.

In recent years, an Australian company, Wave Swell Energy Ltd. (WSE) has been developing a first-of-its-kind wave energy device based on the concept of a unidirectional OWC, which only generates energy on the downstroke, or inhalation phase, of the wave [14]. A 200 kW prototype of the technology, the UniWave200, was installed at King Island in Bass Strait, approximately 100 km off the northwest tip of Tasmania, from 2021 to 2022. WSE's demonstration project was partially funded by a grant from the Australian Renewable Energy Agency (ARENA) and was designed to tangibly demonstrate the technology and to develop skills in designing, building, transporting, deploying, operating, optimizing, and ultimately decommissioning and recycling a full-scale OWC. The project served to optimize the technology's electrical control system and to validate, in actual ocean conditions, the conversion efficiency results obtained in model-scale tests conducted at the University of Tasmania's Australian Maritime College (AMC) in Launceston, Tasmania [15]. A report [16] was prepared on behalf of WSE comparing the performance between the demonstration sea trial at King Island and past model-scale experiments at AMC.

This paper is focused on analyzing and validating the wave-to-grid energy conversion efficiency of the UniWave200in a real-world environment. Section II describes the conditions of the unit's installation, the methods used for data collection during testing, and the industry-standard techniques used to calculate energy conversion efficiency metrics from the measured data. Section III presents the results of an efficiency analysis at each critical energy conversion stage in the generation of electricity from wave to grid. A discussion of the results in comparison to other OWC technologies is presented in Section IV, and conclusions are provided in Section V.

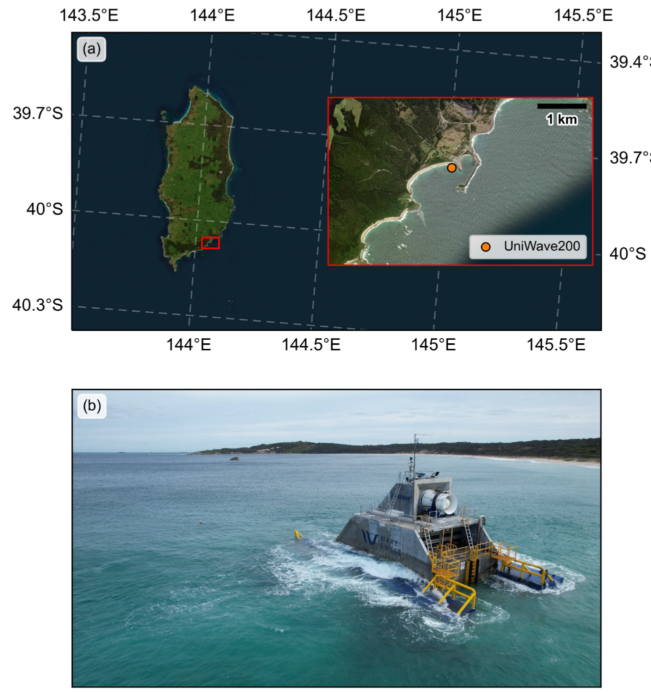

Fig. 1. (a) Map of King Island with an inset showing the deployment location in Grassy Harbour; (b) Photograph of the deployed UniWave200.

II. Methods

A. Device Testing and Data Collection

In January 2021, WSE deployed a 200 kW prototype of its *UniWave* unidirectional OWC technology, the UniWave200, at Grassy Harbour, King Island (Fig. 1). The deployment site for the UniWave200 device was approximately 50 m off Sandblow Beach, adjacent to the harbor of the small town of Grassy.

The UniWave200 is a gravity-based OWC consisting of a reinforced concrete structure with two pontoons—one on either side—that provide the necessary buoyancy for self-installation and decommissioning. The unit is 24 m long and 13.6 m wide, with a chamber length of 4 m and chamber width of 7 m. The unit was installed on a sandy sea bed at a mean sea level depth of 5.1 m. The ballasted mass of the unit was 1080 metric tons. The unit was fitted with 15 bespoke rubber flap air vents and an axial flow air turbine power take-off (PTO) system with a tip diameter equal to 1.29 m, which provided a chamber damping ratio of 1:150. The electrical system consists of a direct current (DC) bus with a supercapacitor energy storage and an active front end (AFE) connected to the King Island electrical grid via a subsea cable and a shore kiosk with breakers and a transformer. A rendering of the UniWave concept is shown in Fig. 2.

Data and measurements were collected using a variety of methods and products. A Beckhoff programmable logic controller (PLC) was responsible for supervisory control and data acquisition (SCADA) activities and was connected to a network attached storage (NAS) system that provided a local PostgreSQL database for data logging. A self-hosted integration run-time instance that was installed on the NAS (running Windows Server 2019) provided access for Azure Data Factory to query the

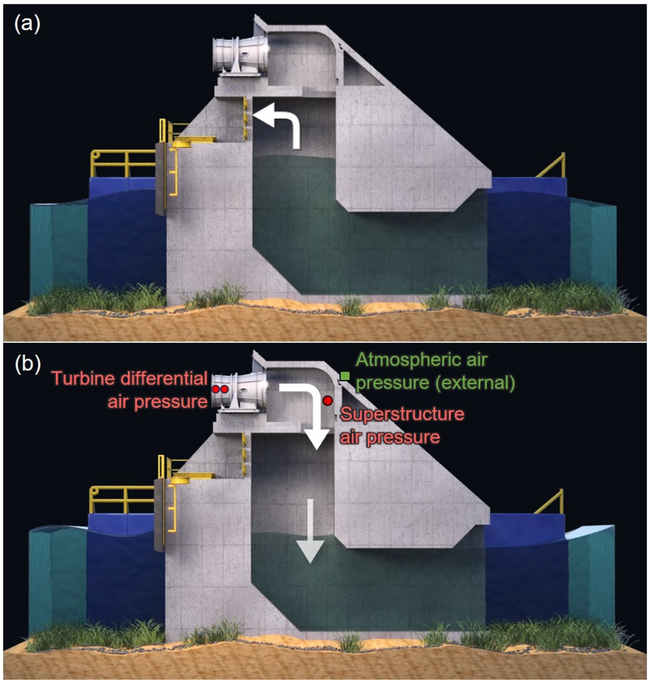

Fig. 2. Rendering of the UniWave concept with white arrows showing the airflows during (a) the upstroke (exhalation/venting) and (b) the downstroke (inhalation/power generation). Red markers in panel (b) show the location of onboard sensors used to compute pneumatic power.

database at half-hour intervals. Queried data were converted to the Parquet format and transferred to Azure blob storage. Near-real-time access to data was possible through the installation of the product TimescaleDB overlaying the PostgreSQL database, which made recent aggregate data (e.g., average, minimum, and maximum) readily accessible.

From July to October 2021, the deployment objectives included commissioning and uptime. Throughout this phase, changes were made to the PLC software to improve the data collection and control settings. While the priority of this initial stage was to have the unit running as often as possible, regardless of the sea state, this priority was later modified during testing to have the unit operating whenever power could be exported. This was nominally defined as when the significant wave height H_s was greater than 0.75 m (from October 2021 to July 2022) and greater than 0.5 m (from July to August 2022). The results presented in this paper are derived from the aggregate data collected from October 2021 to August 2022.

The UniWave200 was instrumented with a variety of sensors used both for operational purposes (such as valve controls) as well as to collect the data necessary for the efficiency analysis presented in this publication, the latter of which are summarized in Table I. The location of the onboard sensors used to compute the pneumatic power is shown in Fig. 2(b) and the locations of the instruments used to measure the incident wave elevation are shown in Fig. 3. The electrical system consisted of a DC bus with supercapacitor energy storage capability and an active front end connected to the King Island electrical grid via a subsea cable to a shore-based kiosk that housed circuit breakers and a transformer.

TABLE I
SUMMARY OF THE INSTRUMENTATION USED TO COLLECT ALL DATA FOR THE EFFICIENCY ANALYSIS

Measured Parameter	Sensor/ Instrument	Range	Accuracy	Sample Rate	Derived Metric for Efficiency Calculations
Wave elevation (from hydraulic pressure)	2 × Keller PAA-36XW (4-20mA)	-3–5 m	0.15%	100 Hz	Wave spectra
Wave elevation (from accelerometer)	Sofar Spotter wave buoy	Varies	±2 cm	2.5 Hz 30 min avg.	Wave bulk parameters (validation only)
Turbine differential air pressure, Δp_{inlet}	2 × Huadian automation HDP704 (4–20 mA)	0–1 kPa	1%	100 Hz	Flow rate for pneumatic power
Superstructure air pressure	2 × Keller PAA-35X (4–20 mA)	50–120 kPa	0.15%	100 Hz	Pneumatic power, Δp
Atmospheric air pressure (external)	2 × Keller PAA-35X (4–20 mA)	90–120 kPa	0.15%	100 Hz	Pneumatic power, Δp
Generator speed	Dynapar B58N	0–3,000 r/min		100 Hz	Turbine mechanical power
PTO system parameters (mechanical torque, voltage, current, power)	Danfoss - Vacon DC/DC converter, AC drive, active front end	Varies		100 Hz	Turbine mechanical power, electrical generated power, electrical exported power
Electrical power	Electrical switchgear	Varies		100 Hz	Electrical generated power, electrical exported power

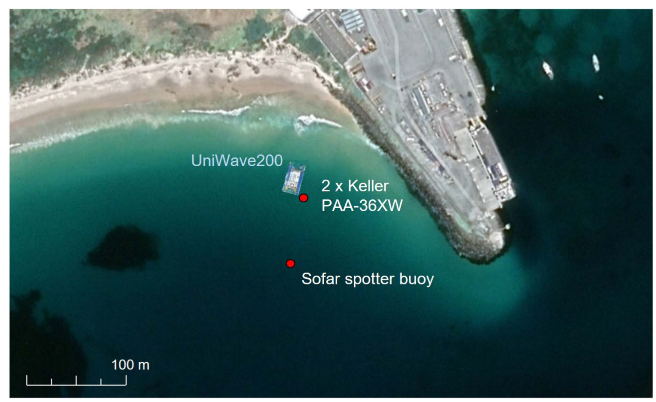

Fig. 3. Location of wave measuring instrumentation near the UniWave200.

B. Data Post-Processing and Validation

Wave elevation is calculated from the dual Keller pressure measurements over three sequential steps. The first step was a hydrostatic approximation used to convert the measured pressure to the hydrostatic head. This approach is suitable for environments such as tanks and containers, including the water level in the UniWave200. The second step involved a linear correction for the attenuation of the pressure signal with depth performed using a fast Fourier transform (FFT) technique as described in [17]. The last step involved a weakly dispersive correction via a spectral analyisis; this approach is suitable for use in the near-shore regions where the waves are weakly dispersive [18] and is the most appropriate choice for the location where the pressure sensors were deployed.

The Keller pressure sensors were located about 20 m away from the UniWave200 relative to the center of the structure. Per the International Electrotechnical Commission Technical Specifications IEC-TS 62600:100 [19], a wave-measuring instrument used in a power performance assessment should be deployed at a location where it can accurately measure the incident wave energy into the tested wave energy converter. Installing sensors too close to the OWC has the potential to corrupt the

TABLE II
ERROR STATISTICS BETWEEN WAVE BULK PARAMETERS DERIVED FROM THE SPOTTER BUOY AND DUAL PRESSURE SENSOR MEASUREMENTS

Parameter	RMSE	PE	b	SI	R
H_s	0.09 m	2.53%	0.01	0.13	0.97
T_p	2.44 s	0.08%	-0.53	0.20	0.67

incident wave signal due to diffraction, radiation, and reflection interaction with the OWC structure itself [20]. In an attempt to determine if this was an issue for the pressure sensors deployed during testing of the UniWave200, a surface-mounted Sofar Ocean Technologies Spotter buoy was installed about 100 m from the center of the OWC (Fig. 1). Unfortunately, the location of the wave spotter was less than a wavelength away from the UniWave200 for about half of the peak wave period range observed during this experiment (peak wave periods between 9 and 20 s corresponding to wave lengths in 5 m water depth of 60 to 140 m), and may have therefore also been affected by diffraction and scattering from the device. While this is less than ideal, the data collected by the spotter buoy is expected to represent wave measurements that are less affected by the device.

Bulk wave parameters (significant wave height and peak period, T_p) derived from the dual pressure sensors and the Spotter buoy datasets were compared through a time series analysis considering commonly used error metrics, including the root-mean-square-error (RMSE), mean percentage error (PE), bias (b), scatter index (SI), and the linear correlation coefficient (R) (see Table II). The equations used to compute these parameters are provided in the Appendix. The time series were compared at a matching time step of 30 min for a total sample size of 8,478 observations. Overall, measurements of the incoming wave taken by the Keller pressure sensors show close agreement to those taken by the Spotter buoy, particularly in terms of the significant wave height, which has an RMSE value of less than 10 cm and an R value of 0.97. Less agreement is observed in the measurement of the peak period, which shows an RMSE value equal to 2.44 s and R equal to 0.67. This can be explained in part by the difference in frequency sampling bins between the instruments, as well as by the filtering effect of the bottom pressure measurement which cannot resolve the short-period energy (as suggested by the negative bias).

While there is general agreement between the two different incident wave datasets, radiation and diffraction effects cannot be ruled out. Studies have shown that these effects can be estimated through potential flow analysis using Boundary Element Method (BEM) models, such as WAMIT or NEMOH [21], [22], [23], [24], or for more accurate results by using Computational Fluid Dynamics (CFD) models [25], [26]. However, developing a potential flow model for an OWC can be particularly challenging because of the nonlinearity effects of the free surface in the chamber [21], [25], while running a CFD model can be considerably more computationally expensive [25], [26]. Such modelling was beyond the scope of this project and for this reason we are unable to quantify the exact magnitude of the error resulting from radiation and diffraction effects implicit in the wave measurements collected.

The water level time series calculated from the hydraulic pressure sensors were used to calculate frequency-resolved variance spectra, S_i, using the Cooley–Tukey algorithm with an applied Hanning window. Additional characteristic wave parameters were computed from the wave spectra following the IEC-TS 62600:100 [19] recommendations. The omnidirectional wave power (J [W/m]), or wave power density, which describes the flux of energy through a unit length, is defined as

$$J = \rho_w g \sum_i c_{g,i} S_i \Delta f_i, \tag{1}$$

where ρ_w is the density of water, g is the gravitational acceleration, c_g is the group velocity as defined by linear wave theory, and f is the discrete frequency. The actual amount of energy entering the mouth of a OWC device is difficult to measure due to non-linear and resonant effects, however, at the mouth of a typical OWC, particularly one in shallow water like the UniWave200, the incident wave is essentially normal to the bathymetry contours and chamber entrance, strongly justifying the use of the omnidirectional wave power for analyzing the hydrodynamic energy efficiency of the device. The significant wave height provides a characteristic wave height of the sea state and is defined as

$$H_s = 4.004\sqrt{m_0}, \tag{2}$$

where m_0 is the zeroth spectral moment derived from the wave variance spectrum:

$$m_n = \sum_i f_i^n S_i \Delta f_i. \tag{3}$$

Lastly, the energy period is presented as a characteristic wave period recommended for wave energy analyses:

$$T_e = \frac{m_{-1}}{m_0}. \tag{4}$$

The pneumatic power (energy flux) at the bell mouth (where the air enters the turbine housing into the atmosphere) was calculated as

$$P_{pneu} = \Delta p Q, \tag{5}$$

where Q is the volumetric flow rate across the turbine and Δp is equal to the atmospheric pressure minus the superstructure air pressure. The atmospheric pressure and the superstructure pressure were each measured by two analogue pressure sensors (dual Keller PAA $\times$ 35 sensors) for added security in the event of instrumentation failures; whenever possible the average of the data recorded by both sensors was used.

Many studies have shown that using orifice plate, or venturi, formulations are effective in calculating the turbine volumetric flow rate in OWC devices [27], [28] as

$$Q = C_d A_o \sqrt{\frac{2\Delta p_{inlet}}{\rho_a}}, \tag{6}$$

where C_d is the orifice discharge coefficient, A_o is the orifice cross-sectional area, Δp_{inlet} is the differential air pressure at the turbine's inlet, and ρ_a is the density of air. The discharge coefficient used in this study comes from a past experiment

TABLE III

NUMBER OF AVAILABLE DATA RECORDS FOR EACH WAVE CONFIGURATION

H_s (m) \ T_e (s)	9	10	11	12	13	14	15	16	17	18	19	20
0.5			1	1								
0.6		4	3	3	1		1	1				
0.7		6	3		2	3	2	6	6	2	3	1
0.8		1	6			4	5	3	3		1	
0.9	1		2	1	2	7	4	3	1	2		
1			1	1	4	4	3	4				
1.1		2	3	2	1	5	3	1	2			
1.2		4	7	2	1	4	1	2				
1.3		6	5	2	1	2	2	1	1			
1.4		1	2		2	5	4	1				
1.5				1	1	1	2					
1.7				1	2							

conducted at the University of Tasmania's AMC of a 1:4 scale model of the Uniwave200 [16]. That experiment involved CFD simulations of varying flow conditions through the scaled turbine using ANSYS CFX 19.1 software and was validated against laboratory experiments of a physical 1:4 scale model of the device. The resulting average value of C_d was of 0.98 with an average error of 0.13% as compared to the physical model tests. This value is consistent with the theoretical expectation that a gently sloping and smooth venturi (i.e., the UniWave200 turbine inlet) minimizes the turbulent flow losses and has therefore a discharge coefficient that approaches unity. The 1:4 scale and full-scale models of the UniWave200 are equivalent based on the principles of Froude number scaling (i.e, geometrical similarity) and we therefore assume the same discharge coefficient of 0.98 for the analysis of the full-scale results. Additionally, the effective flow area of the UniWave200 full-scale turbine is $A_o = 0.54\ \mathrm{m}^2$, and the air density during testing was of $1.18\ \mathrm{kg/m}^3$. The inlet pressure differential was measured between the dual Huadian Automation sensors installed at the turbine's inlet.

C. Analysis Methods

The efficiency of the UniWave200 is analyzed from a collection of 195 files derived from field measurements, each containing 30-min-long time series of the parameters shown in the last column of Table I. Out of the total of 195 data records, 75 different sea states are represented (i.e., unique pairings of H_s and the energy period T_e), achieved by binning the significant wave height in increments of 0.1 m, as shown in Table III. The most common sea states observed correspond to the pairing $H_s = 1.2$ m and $T_e = 11$ s and the pairing $H_s = 0.9$ m and $T_e = 14$ s, with 7 observations of each in the dataset. Sea states characterized by a significant wave height of 1.6 m were not observed during testing.

A sample snapshot of the key measurements collected during one of the most commonly occurring sea states is shown in Fig. 4. Notice that there is a time lag between the wave elevation measurements and the power measurements evidenced by the misalignment of peaks. This is due to the distance between the instrumentation used to collect those data (the pressure sensors used to derive the water elevation are located about 20 m in front of the OWC). In this case, the lag is between 5 and 6 s, but variations in the operating conditions and the sea state do not

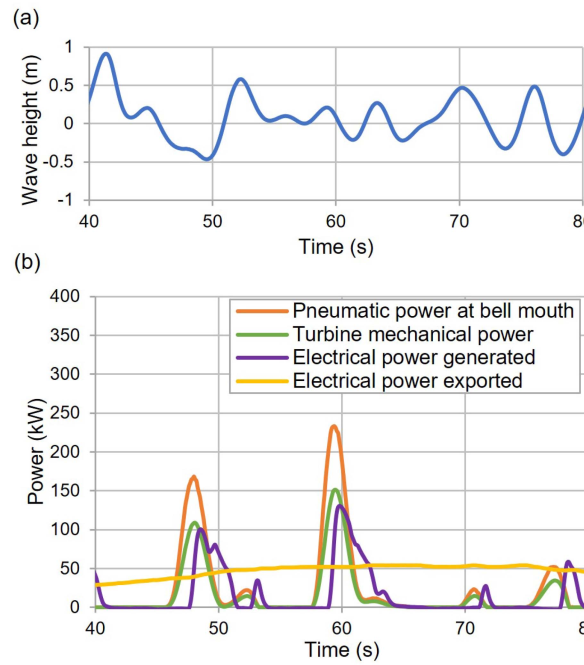

Fig. 4. Time series excerpt (40 s) of (a) the wave height (with the mean water level of 1.4 m subtracted) and (b) power metrics, collected under wave conditions of $H_s = 1.2$ m and $T_e = 11$ s.

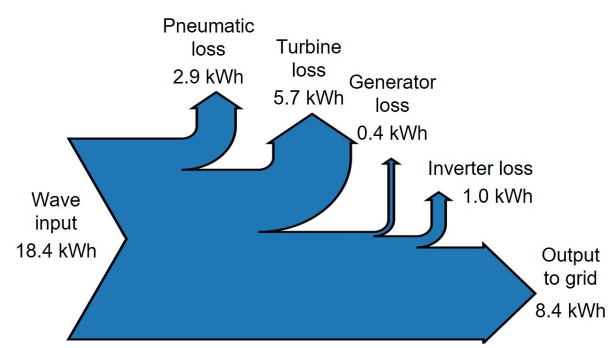

Fig. 5. Sankey diagram of the wave-to-grid energy conversion for a sample sea state of $H_s = 1.2$ m and $T_e = 11$ s.

allow for a simple correction of this lag. A statistical analysis of the ensemble dataset is used to reduce the influence of this time lag. A graphical representation of the stages of wave energy conversion for this sample data record is shown in Fig. 5. The thicknesses of the arrows are sized in proportion with the energy lost at each stage and the total energy exported to the grid. In all cases, energy values (in KWh) were obtained by integrating each 30 min power time series over time using a time step of 0.1 s.

The energy conversion efficiency of the UniWave200 is analyzed using two distinct approaches by (1) computing the bivariate efficiency matrices relative to the significant wave height and wave energy period using only 75 representative data records with unique sea states and (2) generating box and whisker plots of the efficiency relative to the significant wave height using all 195 data records. The first approach is intended to inspect the relationship between unique sea states and efficiency not obscured

TABLE IV
CWR (WAVE-TO-PNEUMATIC EFFICIENCY) MATRIX

	T_e (s)												Median
H_s (m)	9	10	11	12	13	14	15	16	17	18	19	20	Eff (%)
0.5			104.0	88.5									96.2
0.6		94.7	90.9	82.2	60.0		64.8	58.7					84.8
0.7		85.4	85.3		61.4	40.3	58.6	45.1	59.3	43.8	60.8	50.4	61.6
0.8		97.5	92.5			97.6	52.8	66.8	36.6		47.4		70.6
0.9	84.6		94.1	82.9	93.1	81.9	92.6	46.5	56.4	34.8			72.1
1			88.1	95.2	94.3	84.0	77.4	49.1					80.3
1.1		97.5	83.5	80.2	83.4	73.4	83.9	61.9	73.4				79.9
1.2		88.9	78.1	88.4	82.0	70.5	70.1	64.3					81.9
1.3		77.2	79.9	75.7	66.7	76.2	73.0	68.4	71.0				77.9
1.4		101.7	106.4		71.0	67.7	66.2	70.1					69.8
1.5				98.2	100.9	77.0	66.7						76.6
1.7				96.6	66.9								66.9

TABLE V
PTO (PNEUMATIC-TO-GRID) EFFICIENCY MATRIX

	T_e (s)												Median
H_s (m)	9	10	11	12	13	14	15	16	17	18	19	20	Eff (%)
0.5			30.4	24.3									27.4
0.6		32.5	31.7	30.0	18.2		28.1	19.4					31.9
0.7		39.3	40.6		27.5	23.1	36.9	34.0	23.5	20.6	35.8	22.5	34.4
0.8		42.5	48.9			45.7	44.3	42.7	26.5		27.3		44.3
0.9	43.7		45.4	50.3	52.1	52.0	51.9	37.4	45.6	32.0			46.6
1			52.1	54.0	50.3	55.6	52.6	47.1					54.0
1.1		54.7	54.3	53.3	55.7	54.3	54.9	51.9	55.2				55.9
1.2		53.6	54.3	53.9	55.8	59.8	60.0	56.3					57.7
1.3		55.0	55.5	56.5	56.8	54.8	56.7	59.8	59.6				58.7
1.4		59.0	56.7		59.9	58.7	58.5	57.3					61.4
1.5				59.1	59.1	58.7	60.4						61.9
1.7				59.9	61.5								63.5

TABLE VI
WAVE-TO-GRID EFFICIENCY MATRIX

	T_e (s)												Median
H_s (m)	9	10	11	12	13	14	15	16	17	18	19	20	Eff (%)
0.5			31.6	21.5									26.4
0.6		30.8	28.8	24.6	10.9		18.2	11.4					28.9
0.7		33.6	34.6		16.9	9.3	21.7	15.3	14.0	9.0	21.8	11.3	21.0
0.8		41.4	45.2			44.6	23.4	28.6	9.7		12.9		31.9
0.9	36.9		42.7	41.7	48.5	42.6	48.0	17.4	25.7	11.1			34.2
1			45.8	51.4	47.5	46.7	40.7	23.1					45.7
1.1		53.3	45.3	42.8	46.5	39.9	46.1	32.1	40.6				43.3
1.2		47.7	42.4	47.7	45.8	42.2	42.1	36.2					47.4
1.3		42.5	44.4	42.8	37.8	41.8	41.4	40.9	42.3				45.5
1.4		60.1	60.3		42.5	39.8	38.8	40.2					43.4
1.5				58.0	59.7	45.2	40.2						48.1
1.7				57.9	41.2								44.5

by outliers, while the second approach highlights the variance in efficiency for all sample records, including statistical outliers. The conversion efficiency analysis is focused on two stages of energy conversion: a) wave-to-pneumatic characterized from the capture width ratio (CWR), b) pneumatic-to-grid based on the combined elements of the PTO system (turbine, generator and inverter); and the combined CWR and PTO total efficiency: c) wave-to-grid.

First, the efficiency of the wave-to-pneumatic energy conversion is typically evaluated through the CWR [11], [29] which is a measure of the hydrodynamic absorption of the input wave energy defined as

$$CWR[\%] = \frac{P_{pneu}}{JB} \times 100, \tag{7}$$

where B is the characteristic dimension of the WEC, which for an OWC is usually equated to the chamber width (7 m for the UniWave200). The length of the OWC chamber, while important for assessing the effects of resonance, is not a relevant parameter when analyzing the absorption efficiency of the incident energy.

Second, the pneumatic-to-grid energy conversion is achieved by the combined elements of the PTO system. This includes the sequential conversion of the bell mouth pneumatic energy to the turbine mechanical energy, then of mechanical energy to electric energy produced by the generator, and finally a transfer of electricity exported to the grid via the inverter. The pneumatic-to-grid efficiency, or PTO efficiency, is calculated by multiplying the turbine efficiency, generator efficiency, and inverter efficiency, which are computed as

- Turbine efficiency = Turbine mechanical energy/Pneumatic energy at the bell mouth,
- Generator efficiency = Electrical energy generated/Turbine mechanical energy,
- Inverter efficiency = Electrical energy exported/Electrical energy generated.

Third, the total wave-to-grid efficiency is defined as the product of the wave-to-pneumatic efficiency as described by the CWR and the pneumatic-to-grid efficiency as described by the PTO efficiency.

III. RESULTS

A. *Efficiency Analysis*

The energy conversion efficiency matrices are based on 75 representative records of unique sea states, or H_s and T_e combinations. Tables IV, V, and VI show the CWR (wave-to-pneumatic), PTO efficiency (pneumatic-to-grid), and wave-to-grid efficiency matrices, respectively, with efficiency values shown as percentages. The last column on the right of each matrix shows the median efficiency corresponding to each discrete significant wave height accounting for all 195 data records (as opposed to only 75).

The CWR bivariate matrix (Table IV) is most variable for low values of the significant wave height, with minimum and maximum median values of 61.6% and 96.2%, respectively. The overall median CWR is 74.1%. Another observation is that there are some instances of CWR values above 100%. This could be due to various contributing factors including wave reflections from the beach or the WEC structure itself, the phase lag between the wave measurements and other power measurements, and resonance driven by the interaction of the incoming waves with the device.

The PTO efficiency matrix (Table V) shows a lower efficiency at lower values of the significant wave height, with a minimum median efficiency of 27.4% for $H_s = 0.5$ m and a maximum median efficiency of 63.5% for $H_s = 1.7$ m. A noticeable increase in the efficiency is observed with increasing values of significant wave height in the range of 0.5–1.2 m, after which the WEC starts to approach a maximum efficiency point, possibly due to the limitations of the turbine and inverter system.

The wave-to-grid efficiency matrix (Table VI) shows a general trend of increased efficiency with increasing significant wave height, with a minimum median efficiency of 21.0% for $H_s = 0.7$ m and a maximum median efficiency of 48.1% for $H_s = 1.5$ m.

The distributions of the efficiency at each conversion stage for discrete values of the significant wave height, considering all 195 data records rather than unique sea states, are analyzed using box-and-whisker plots (Fig. 6). The rectangular box of a box-and-whisker plot represents the interquartile range (IQR) from the 25th percentile (also known as the first quartile or Q1) up to the 75th percentile (also known as the third quartile or Q3). The lower whiskers represent the data points from Q1 − 1.5 × IQR up to Q1, while the top whiskers represent the data points from Q3 up to Q3 + 1.5 × IQR. Any data points outside the range of the whiskers are outliers represented by the small circles. The

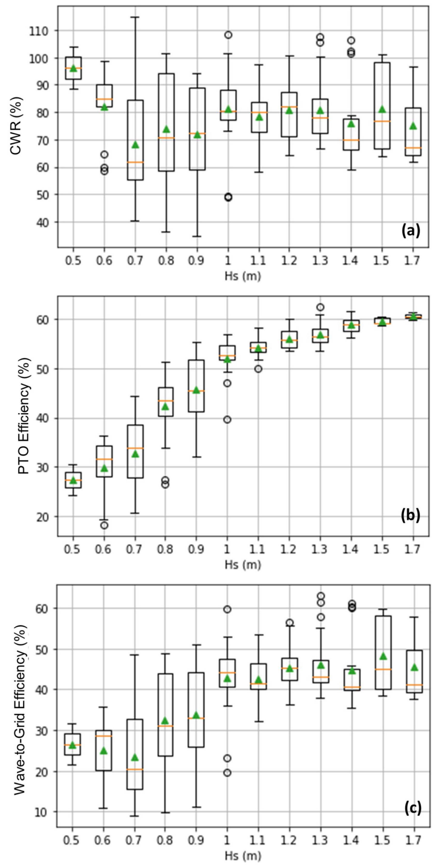

Fig. 6. Distributions of the (a) CWR (wave-to-pneumatic efficiency), (b) PTO (pneumatic-to-grid) efficiency, and (c) wave-to-grid efficiency for discrete values of the significant wave height.

median and mean of each distribution are represented by orange horizontal lines and green triangles, respectively.

For each value of H_s, the hydrodynamic efficiency (CWR) (Fig. 6(a)) shows greater variance than that of the PTO efficiency (Fig. 6(b)). The lack of a trend between the CWR and the significant wave height suggests that other wave parameters, such as the wave period, may significantly impact the efficiency at the first conversion stage. In contrast, in Fig. 6(b), we observe a trend of increasing PTO efficiency associated with increasing H_s, indicating that wave height is a significant factor in the pneumatic-to-grid conversion process (which includes the turbine, generator, and inverter all together).

Increasing wave heights are associated with a greater PTO efficiency because the unit is more likely to operate near the rated capacity of the power electronics in more energetic sea states. Additionally, the supercapacitor experiences significant charging in strong seas, enabling discharge for a longer period and reducing the variability in efficiency. Meanwhile, at lower-energy sea states, the energy loss within the components represents a higher percentage of the energy harvested.

IV. Discussion

The wide range of ocean conditions experienced by the UniWave200 device was an important part of WSE's strategy for testing the unit in as diverse a set of conditions as possible. The dimensions of the OWC were designed for swell periods of approximately 12 s, and although such conditions were encountered regularly, the unit was exposed to periods ranging from 9 to 20 s. The topographic features in the vicinity of the site (small islands and rocky outcrops, the adjacent breakwater, etc.) likely attenuated the energy of incoming swell waves. It can be expected that such a device will be located in locations with more uniform topography in the future and will therefore experience more regular and uniform swell conditions. As a result, the conversion efficiencies may be higher than those described in this paper.

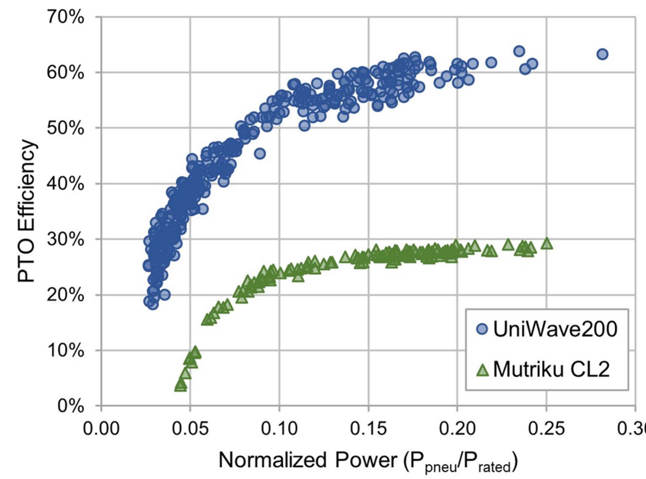

Fig. 7. PTO efficiency distributions versus the normalized pneumatic power of the UniWave200 and Mutriku.

The CWR of a given category of WEC (e.g., heaving, overtopping) is often estimated as a measure of hydraulic efficiency from the regression equations derived by Babarit [11] which are based on model tests, sea trials, and numerical modeling of various WEC concepts in the industry (although numerical data is not considered for OWCs in particular). The best fit equation of the CWR for OWC devices has a skill of $R^2 = 0.69$ and is reported in Table 11 of [11] as a function of the characteristic dimension B—a parameter consistently set equal to the chamber width. Computing the regression equation for $B = 7$ m (the chamber width of the UniWave200) results in a CWR of $12\% \pm 56\%$ or a maximum efficiency with a 95% level of confidence of 68%. The UniWave200 surpasses this estimate with an overall median CWR (wave-to-pneumatic efficiency) of 74.1%, and was also shown to have a minimum median CWR of 61.6% (for significant wave heights of 0.7 m) that is on the upper end of the Babarit range. The regression equation was based on datasets corresponding to bidirectional OWC technologies, which may indicate that more power is able to be extracted from a unidirectional OWC than is possible via a similar bidirectional counterpart.

For an additional assessment against other documented OWC technologies, we compare the PTO (pneumatic-to–grid) efficiency of the UniWave200 to the Mutriku OWC (Fig. 7). The PTO efficiency values for Mutriku were reported by Fay et al. in Fig. 32(c) of [12] and were digitized using the open-source

MATLAB toolbox GRABIT [30]. The pneumatic power values were normalized by dividing them by the rated power of each device's PTO system for a fair comparison. This figure suggests that the UniWave200 PTO performs with up to 30% greater absolute efficiency than the Mutriku PTO (approximately 100% greater relative efficiency). Note that this is not a direct comparison of the CWR or wave-to-grid total efficiency between these technologies.

V. Conclusion

A 200 kW unidirectional OWC WEC developed by WSE, known as the UniWave200, was deployed for testing during a grid-connected demonstration project off the coast of King Island, Tasmania, Australia. Data were collected in 30 min bursts, amounting to 195 records of wave and various power measurements. The sea states observed during testing encompassed significant wave heights ranging from 0.5 to 1.7 m and energy periods ranging from 9 to 20 s.

During the first phase of the energy conversion process, from wave to pneumatic energy, the median value of the capture width ratio, calculated as a proxy of hydrodynamic absorption efficiency, was found to be equal to 74.1%, showing greatest variance for significant wave heights under 1 m.

The PTO efficiency, representing the second phase of the energy conversion process from pneumatic energy to electric energy exported to the grid, generally increased with increasing wave heights resulting in a median efficiency of 48.8%. The lower efficiency for smaller waves is likely the result of the onboard electrical infrastructure being overrated at these low power levels. The trend of higher efficiency for larger waves may imply higher average energy production at commercial wave sites likely to experience larger waves more frequently.

Lastly, the wave-to-grid efficiency, or total efficiency, has an overall median value of 36.9%. The median efficiency for H_s values up to 0.8 m was about 30% or less, with average efficiencies above 50% becoming more typical for sea states with a significant wave height above 1.5 m.

The fact that the UniWave200 unit tends to perform better for larger wave heights would appear to be a positive for the technology. Commercial versions of the technology are likely to be sited in more energetic (less sheltered) wave regions where H_s values above 1.0 m will be more common. However, as energetic sea states at the high end of a typical range for a commercial wave energy site were not observed during the test deployment, performance could not be determined for such conditions. These results may be a valuable tool for validating numerical models and simulating performance in alternate conditions.

Appendix
Definition of Error Metrics

The statistical metrics used to evaluate the error in field measurements are the root-mean-square-error (RMSE), mean percentage error (PE), bias (b), scatter index (SI), and the linear correlation coefficient (R). These parameters are defined as

$$RMSE = \sqrt{\frac{\sum_{i=1}^{N}(\hat{y}_i - y_i)^2}{N}}, \tag{8}$$

$$PE = \frac{100}{N}\sum_{i=1}^{N}\frac{\hat{y}_i - y_i}{y_i} \tag{9}$$

$$b = \frac{1}{N}\sum_{i=1}^{N}\hat{y}_i - y_i \tag{10}$$

$$SI = \frac{RMSE}{\overline{y}} \tag{11}$$

$$R = \frac{\sum_{i=1}^{N}(\hat{y}_i - \overline{\hat{y}})(y_i - \overline{y})}{\sqrt{[\sum_{i=1}^{N}(\hat{y}_i - \overline{\hat{y}})^2][\sum_{i=1}^{N}(y_i - \overline{y})^2]}} \tag{12}$$

where N is the total number of observations, $\hat{y}_i$ is the measured value for the *i-th* observation recorded by the Keller pressure sensors, y_i is the measured data recorded by the Sofar Spotter buoy considered here to represent the *true* values, and overlines represent time averages.

Acknowledgment

The authors would like to thank Alan Fleming and Alan Henderson, from the Australian Maritime College at the University of Tasmania, for providing technical input on the experimental design of the field test at King Island and associated laboratory experiments and numerical simulations. The authors also thank Gabriel García Medina and Sarmad Hanif, formerly with Pacific Northwest National Laboratory, for their contributions to the initial data analysis presented in this publication. PNNL's independent analysis and conclusions are based entirely on the information and data provided by WSE. This publication does not necessarily constitute or imply an endorsement, recommendation, or favoring by the United States Government.

References

[1] B. G. Reguero, I. J. Losada, and F. J. Méndez, "A global wave power resource and its seasonal, interannual and long-term variability," *Appl. Energy*, vol. 148, pp. 366–380, 2015.
[2] K. Gunn and C. Stock-Williams, "Quantifying the global wave power resource," *Renewable Energy*, vol. 44, pp. 296–304, 2012.
[3] S. Ahn, V. S. Neary, and K. A. Haas, "Global wave energy resource classification system for regional energy planning and project development," *Renewable Sustain. Energy Rev.*, vol. 162, 2022, Art. no. 112438.
[4] B. Guo and J. V. Ringwood, "A review of wave energy technology from a research and commercial perspective," *IET Renewable Power Gener.*, vol. 15, no. 14, pp. 3065–3090, 2021.
[5] A. F. O. de Falcao, "Wave energy utilization: A review of the technologies," *Renewable Sustain. Energy Rev.*, vol. 14, no. 3, pp. 899–918, 2010.
[6] A. F. O. Falcão and J. C. C. Henriques, "Oscillating-water-column wave energy converters and air turbines: A review," *Renewable Energy*, vol. 85, pp. 1391–1424, 2016.
[7] L. M. C. Gato and M. Webster, "An experimental investigation into the effect of rotor blade sweep on the performance of the variable-pitch wells turbine," *Proc. Inst. Mech. Engineers, Part A: J. Power Energy*, vol. 215, no. 5, pp. 611–622, 2001.
[8] L. M. C. Gato, V. Warfield, and A. Thakker, "Performance of a high-solidity wells turbine for an OWC wave power plant," *J. Energy Resour. Technol.*, vol. 118, no. 4, pp. 263–268, 1996.
[9] T. Setoguchi, S. Santhakumar, M. Takao, T. H. Kim, and K. Kaneko, "A modified wells turbine for wave energy conversion," *Renewable Energy*, vol. 28, no. 1, pp. 79–91, 2003.
[10] D. N. Ferreira, L. M. C. Gato, and L. Eça, "Efficiency of biradial impulse turbines concerning rotor blade angle, guide-vane deflection and blockage," *Energy*, vol. 266, 2023, Art. no. 126390.
[11] A. Babarit, "A database of capture width ratio of wave energy converters," *Renewable Energy*, vol. 80, pp. 610–628, 2015.

[12] F.-X. Fay, E. Robles, M. Marcos, E. Aldaiturriaga, and E. F. Camacho, "Sea trial results of a predictive algorithm at the Mutriku Wave power plant and controllers assessment based on a detailed plant model," *Renewable Energy*, vol. 146, pp. 1725–1745, 2020.

[13] A. F. O. Falcão, A. J. N. A. Sarmento, L. M. C. Gato, and A. Brito-Melo, "The Pico OWC wave power plant: Its lifetime from conception to closure 1986–2018," *Appl. Ocean Res.*, vol. 98, 2020, Art. no. 102104.

[14] N. Ansarifard, S. S. Kianejad, A. Fleming, A. Henderson, and S. Chai, "Design optimization of a purely radial turbine for operation in the inhalation mode of an oscillating water column," *Renewable Energy*, vol. 152, pp. 540–556, 2020.

[15] A. Fleming, G. MacFarlane, S. Hunter, and T. Denniss, "Power performance prediction for a vented oscillating water column wave energy converter with a unidirectional air turbine power take-off," in *Proc. 12th Eur. Wave Tidal Energy Conf.*, Cork, Ireland, 2017, pp. 1–7. [Online]. Available: https://hdl.handle.net/102.100.100/523444

[16] A. Fleming and G. MacFarlane, "UniWave200 full scale and 1:16 scale performance comparison–condensed version," AMC Search, Australian Maritime College, Tasmania, Australia, 22/M/01 (A), Oct. 2022.

[17] D. T. Gibbons, G. Jones, E. Siegel, A. Hay, and F. Johnson, "Performance of a new submersible tide-wave recorder," in *Proc. OCEANS MTS/IEEE*, 2005, pp. 1057–1060.

[18] A. Mouragues, P. Bonneton, D. Lannes, B. Castelle, and V. Marieu, "Field data-based evaluation of methods for recovering surface wave elevation from pressure measurements," *Coastal Eng.*, vol. 150, pp. 147–159, Aug. 2019.

[19] IEC, "Part 100: Electricity producing wave energy converters - power performance assessment," Int. Electrotechnical Commission, Geneva, Switzerland, Tech. Specification 62600-100:2012, 2012.

[20] J. Berque et al., "Wave energy measurement methodologies for IEC technical specifications" OPERA Open Sea Operating Experience to Reduce Wave Energy Costs, Report D5.1, 2016. [Online]. Available: https://repository.oceanbestpractices.org/handle/11329/1000

[21] M. Penalba, T. Kelly, and J. V. Ringwood, "Using NEMOH for modelling wave energy converters: A comparative study with WAMIT," in *Proc. 12th Eur. Wave Tidal Energy Conf.*, Cork, Ireland, 2017.

[22] H. B. Bingham, D. Ducasse, K. Nielsen, and R. Read, "Hydrodynamic analysis of oscillating water column wave energy devices," *J. Ocean Eng. Mar. Energy*, vol. 1, no. 4, pp. 405–419, Nov. 2015, doi: 10.1007/s40722-015-0032-4.

[23] B. Joensen, H. B. Bingham, R. W. Read, K. Nielsen, and J. B. Trevino, "Hydrodynamic analysis of one-way energy capture by an oscillating water column wave energy device," *Energy Rep.*, vol. 9, pp. 5306–5322, Dec. 2023. [Online]. Available: https://www.sciencedirect.com/science/article/pii/S2352484723004122

[24] M. Rosati, J. C. C. Henriques, and J. V. Ringwood, "Oscillating-water-column wave energy converters: A critical review of numerical modelling and control," *Energy Convers. Manage.: X*, vol. 16, 2022, Art. no. 100322. [Online]. Available: https://www.sciencedirect.com/science/article/pii/S2590174522001453

[25] M. Penalba, G. Giorgi, and J. V. Ringwood, "Mathematical modelling of wave energy converters: A review of nonlinear approaches," *Renewable Sustain. Energy Rev.*, vol. 78, pp. 1188–1207, Oct. 2017. [Online]. Available: https://www.sciencedirect.com/science/article/pii/S1364032116308784

[26] F. Opoku, M. N. Uddin, and M. Atkinson, "A review of computational methods for studying oscillating water columns–the Navier-Stokes based equation approach," *Renewable Sustain. Energy Rev.*, vol. 174, 2023, Art. no. 113124. [Online]. Available: https://www.sciencedirect.com/science/article/pii/S136403212201005X

[27] A. Fleming and G. Macfarlane, "In-situ orifice calibration for reversing oscillating flow and improved performance prediction for oscillating water column model test experiments," *Int. J. Mar. Energy*, vol. 17, pp. 147–155, Apr. 2017. [Online]. Available: https://www.sciencedirect.com/science/article/pii/S221416691730005X

[28] J. Orphin, P. Schmitt, J.-R. Nader, and I. Penesis, "Experimental investigation into laboratory effects of an OWC wave energy converter," *Renewable Energy*, vol. 186, pp. 250–263, Mar. 2022. [Online]. Available: https://www.sciencedirect.com/science/article/pii/S096014812101819X

[29] A. Ulazia, M. Penalba, G. Ibarra-Berastegui, J. Ringwood, and J. Sáenz, "Reduction of the capture width of wave energy converters due to long-term seasonal wave energy trends," *Renewable Sustain. Energy Rev.*, vol. 113, 2019, Art. no. 109267. [Online]. Available: https://www.sciencedirect.com/science/article/pii/S1364032119304757

[30] Jiro Doke, "GRABIT," MATLAB central file exchange, Nov. 2023. [Online]. Available: https://www.mathworks.com/matlabcentral/fileexchange/7173-grabit

Fadia Ticona Rollano received the B.S. degree in civil engineering from the University of Kansas, Lawrence, KS, USA, in 2014, and the M.S. degree in civil engineering, with a focus on ocean and coastal engineering from Oregon State University, Corvallis, OR, USA, in 2018. In 2019, she joined the Pacific Northwest National Laboratory's Coastal Sciences Division, Seattle, WA, USA. Her research interests include applications of marine energy technologies in small- to grid-scale projects and wave and ocean modeling for energy resource characterization. Ms. Ticona Rollano is a Registered Professional Engineer in the State of Washington.

Arthur Santos received the B.S. degree in electrical engineering from the Federal Center for Technological Education of Minas Gerais, Brazil, in 2007, and the M.S. and Ph.D. degrees in electrical and computer engineering and systems engineering from Colorado State University, Fort Collins, CO, USA, in 2020 and 2022, respectively. He is currently a Research Scientist with the CSU Energy Institute,Fort Collins, CO, and is focused on modeling oil and gas facilities with the aim of accurately estimating methane emissions. Arthur is actively engaged in addressing the challenges associated with reconciling bottom-up and top-down methane emissions estimates.

Robert J. Cavagnaro (Member, IEEE) received the B.S. degree in mechanical engineering from Carnegie Mellon University, Pittsburgh, PA, USA, in 2007, and the M.S. and Ph.D. degrees in mechanical engineering from the University of Washington, Seattle, WA, USA, in 2012 and 2016, respectively. He is currently a Mechanical Engineer and Subsector Lead with Pacific Northwest National Laboratory's Marine and Coastal Research Laboratory, Sequim, WA, USA, focused on the advancement of marine energy and robotics technologies.

Scott Hunter received the Bachelor of Engineering (Naval Architecture) degree from the University of New South Wales, Sydney, NSW, Australia, in 2002. He has been involved in the design, development, and operation of marine renewable technologies in Australia, Europe, and the USA for more than 20 years.

Tom Denniss received the B.Math. degree from the University of Wollongong, Wollongong, NSW, Australia, in 1983, the B.Sc. degree (with Hons class 1) from the University of New South Wales (UNSW), Sydney, NSW, Australia, in 1990, and the Ph.D. degree in mathematics from UNSW in 1995, focusing on physical oceanography. He has worked at universities and in investment banking prior to cofounding Wave Swell Energy Ltd. in 2016.